

On the Imperfection Sensitivity of Thin-Walled Frames

S. Gabriele, N. Rizzi and V. Varano
Università degli Studi Roma Tre
Rome, Italy

Abstract

The analysis of two L-frames made up by channel sections subjected to various constraint conditions has been performed in order to determine their buckling and post-buckling behaviour. The analysis has been carried out in the framework of the asymptotic bifurcation theory, using a one-dimensional nonlinear elastic beam model able to account for warping. For each case considered, the first two buckling loads have been determined, together with the associated eigenmodes. For the frames showing an asymmetric postbuckling behaviour only the initial slope of the bifurcated path has been determined. In case of symmetric behaviour, also the secondary modes and the initial curvatures of the bifurcated path have been evaluated. The effects of small initial imperfections have also been studied in order to estimate the real load carrying capacity of the frames for all the cases examined.

Keywords: thin-walled structures, flexural-torsional buckling, Koiter theory, imperfection sensitivity.

1 Introduction

Due to their lightness associated to a relevant strength, Thin Walled Beams are largely used in many structural applications.

The most relevant feature of those structure is that, when subjected to torsion, their cross sections show an out of plane deformation (warping) that, depending on their shape, can be very large.

The technical relevance of this phenomenon was pointed out at the beginning of the XXth century in the pioneering works of Wagner [1] and Kappus [2] and widely investigated by Vlasov[3]. Since then the analysis of the structural behaviour of TWBs has received a constant attention by many researchers whose works have largely increased

our knowledge in the field.

Recently [4], [5], two of the authors have studied the effects of warping constraints together with its transmission across the joints, on the buckling and postbuckling behaviour of frames made up by TWBs.

The analysis performed in the cited papers has been focused on frames showing an asymmetric postbuckling behaviour and has been limited to evaluate the initial slope of the bifurcated paths.

Now, although the asymmetric behaviour leads, in general, to an imperfection sensitivity which is much higher than that shown by frames with symmetric postbuckling behaviour, this can not be assumed as a rule.

In this paper, using a nonlinear 1D beam model which accounts for warping and asymmetry of the cross sections [6] and the tools of the asymptotic bifurcation theory due to Koiter [7], [8] two L-frames showing asymmetric and symmetric bifurcated paths are analyzed.

In order to make a comparison of some of the results obtained, the frames are made up by channel beams having the same length and cross sections of those of the L-frame analyzed by Basaglia et al. [9] in the framework of the GBT theory. In the case of asymmetric behaviour the analysis, as usual, ends with the assessment of the initial postbuckling slope of the bifurcated path. In case of symmetric behaviour, instead, the initial curvature is also determined.

All the analyses have been performed by regarding the structures as *perfect*. The assessment of their imperfection sensitivity has been accomplished in a second step.

To this end, it must be stressed that the asymptotic approach proves to be a very effective tool. In fact, once the *perfect* structure has been examined, then the evaluation of the equilibrium path resulting from an assigned imperfection, can be determined in a very straightforward way together with the load carrying capacity of the structure. This allows to consider the response of the studied frames when subjected of a number of possible initial imperfections, in a very easy way.

The numerical results obtained show how the arrangement of the beams, the constraint on the out of plane sway of the joint and the warping transmission across it, can affect the load carrying capacity of the frame.

Finally we want to remark that, although the asymptotic theory, in general, is not able to describe the bifurcated equilibrium paths far from the neighborhood of the critical load, when the problem at hand is given an adequate nonlinear model, it gives a very good approximation of the imperfection sensitivity of the structures with a limited computational effort.

2 A direct one-dimensional model for thin-walled beams

In this section we give a short account of the 1D model adopted in the analysis. For more details, the reader is referred to [4] and [6].

Let us consider a plane cross-section and denote by o and c its centroid and shear center, respectively. We can think to orthogonally attach a section to each point of a straight line of length ℓ , that we call the beam axis. In particular, we consider the cases in which the axis is the line of the centroids or, alternatively, the line of the shear centers. We fix orthogonal cartesian co-ordinates with x_1 parallel to the beam axes and a consistent ortho-normal right-handed vector basis $(\mathbf{i}_1, \mathbf{i}_2, \mathbf{i}_3)$. Suitable strain measures [10, 11] are

$$\begin{aligned}
\mathbf{E} &= \mathbf{R}^\top \mathbf{R}' = \chi_1 \mathbf{i}_2 \wedge \mathbf{i}_3 + \chi_2 \mathbf{i}_3 \wedge \mathbf{i}_1 + \chi_3 \mathbf{i}_1 \wedge \mathbf{i}_2, \\
\mathbf{e}_o &= \mathbf{R}^\top \mathbf{p}'_o - \mathbf{q}'_o = \varepsilon_1 \mathbf{i}_1 + \varepsilon_2 \mathbf{i}_2 + \varepsilon_3 \mathbf{i}_3, \\
\mathbf{e}_c &= \mathbf{R}^\top \mathbf{p}'_c - \mathbf{q}'_c = \mathbf{e}_o + \mathbf{E} \mathbf{c} = \varepsilon_{1c} \mathbf{i}_1 + \varepsilon_{2c} \mathbf{i}_2 + \varepsilon_{3c} \mathbf{i}_3 \\
&= (\varepsilon_1 + \chi_2 c_3 - \chi_3 c_2) \mathbf{i}_1 + (\varepsilon_2 - \chi_1 c_3) \mathbf{i}_2 + (\varepsilon_3 + \chi_1 c_2) \mathbf{i}_3, \\
\alpha, \quad \eta &= \alpha',
\end{aligned} \tag{1}$$

where: $\mathbf{c} = c - o = c_2 \mathbf{i}_2 + c_3 \mathbf{i}_3$; $\mathbf{p}_o(x_1, t)$, $\mathbf{p}_c(x_1, t)$ are the vector-valued functions describing the present placements of the axes given by $\mathbf{q}_o(x_1)$ and $\mathbf{q}_c(x_1)$ in the reference shape; $\mathbf{R}(x_1, t)$ is the proper orthogonal tensor-valued cross-sections rotation from the reference to the present shape; and $\alpha(x_1, t)$ is a scalar-valued function that we consider as a coarse descriptor of warping. Besides, χ_1 stands for the torsion curvature (twist) and χ_2, χ_3 for the bending curvatures; ε_1 is the elongation of the centroidal axis, $\varepsilon_2, \varepsilon_3$ are the shearing strains between this axis and the cross-section planes; $\varepsilon_{1c}, \varepsilon_{2c}, \varepsilon_{3c}$, are the same quantities referred to the axis of the shear centers.

The displacement of the points belonging to the centroidal and shear center axes together with the rotation are given the following component form

$$\begin{aligned}
\mathbf{u} &= \mathbf{p}_o - \mathbf{q}_o = u_1 \mathbf{i}_1 + u_2 \mathbf{i}_2 + u_3 \mathbf{i}_3 \\
\mathbf{u}_c &= \mathbf{p}_c - \mathbf{q}_c = u_{1c} \mathbf{i}_1 + u_{2c} \mathbf{i}_2 + u_{3c} \mathbf{i}_3
\end{aligned} \quad \mathbf{R} = \mathbf{R}_3 \mathbf{R}_2 \mathbf{R}_1 \tag{2}$$

where \mathbf{R}_1 is a rotation of amplitude θ_1 around \mathbf{i}_1 ; \mathbf{R}_2 is a rotation of amplitude θ_2 around $\mathbf{R}_1 \mathbf{i}_2$; \mathbf{R}_3 is a rotation of amplitude θ_3 around $\mathbf{R}_2 \mathbf{R}_1 \mathbf{i}_3$.

By substituting (2) in (1) one obtains nonlinear strain–displacements relationships that we synthetically refer to in the form

$$\boldsymbol{\epsilon} = e(u) \tag{3}$$

We assume that the beam is homogeneous, nonlinearly hyperelastic, and that its elastic energy density, expressed in terms of the strain components $\varepsilon_{1c}, \varepsilon_{2c}, \varepsilon_{3c}, \chi_1, \chi_2, \chi_3, \alpha, \eta$, is

$$\begin{aligned}
\varphi = & \frac{1}{2}a(\varepsilon_{1c} - c_3\chi_2 + c_2\chi_3)\varepsilon_{1c} + \frac{1}{4}d\chi_1^2\varepsilon_{1c} \\
& + \frac{1}{2}b_2\chi_2^2 + \frac{1}{4}(f_2 - c_3d)\chi_1^2\chi_2 - \frac{1}{2}c_3a(\varepsilon_{1c} - c_3\chi_2 + c_2\chi_3)\chi_2 \\
& + \frac{1}{2}b_3\chi_3^2 + \frac{1}{4}(f_3 + c_2d)\chi_1^2\chi_3 + \frac{1}{2}c_2a(\varepsilon_{1c} - c_3\chi_2 + c_2\chi_3)\chi_3 \\
& + \frac{1}{2}c\chi_1^2 + \frac{1}{4}(f_2\chi_2 + f_3\chi_3 + g\eta)\chi_1^2 + \frac{1}{4}d(\varepsilon_{1c} - c_3\chi_2 + c_2\chi_3)\chi_1^2 \\
& + \frac{1}{2}g_2\varepsilon_{2c}^2 + \frac{1}{2}g_3\varepsilon_{3c}^2 \\
& + \frac{1}{2}h\eta^2 + \frac{1}{4}g\chi_1^2\eta + \frac{1}{2}k(\alpha - \xi\chi_1)^2
\end{aligned} \tag{4}$$

Making the derivative of φ with respect to the strain components, the following stress measures are obtained

$$\begin{aligned}
Q_1 &= \frac{\partial\varphi}{\partial\varepsilon_{1c}} = a(\varepsilon_{1c} + c_2\chi_3 - c_3\chi_2) + \frac{1}{2}d\chi_1^2 \\
Q_2 &= \frac{\partial\varphi}{\partial\varepsilon_{2c}} = g_2\varepsilon_{2c} \\
Q_3 &= \frac{\partial\varphi}{\partial\varepsilon_{3c}} = g_3\varepsilon_{3c} \\
S_1 &= \frac{\partial\varphi}{\partial\chi_1} = c\chi_1 + (d\varepsilon_{1c} + f_2\chi_2 + f_3\chi_3 + g\eta)\chi_1 + c_2d\chi_1\chi_3 - c_3d\chi_1\chi_2 - \xi\tau \\
S_2 &= \frac{\partial\varphi}{\partial\chi_2} = b_2\chi_2 + \frac{1}{2}f_2\chi_1^2 - c_3Q_1 \\
S_3 &= \frac{\partial\varphi}{\partial\chi_3} = b_3\chi_3 + \frac{1}{2}f_3\chi_1^2 + c_2Q_1 \\
\tau &= \frac{\partial\varphi}{\partial\alpha} = k(\alpha - \xi\chi_1) \\
\mu &= \frac{\partial\varphi}{\partial\eta} = h\eta + \frac{1}{2}g\chi_1^2
\end{aligned} \tag{5}$$

$Q_1, Q_2, Q_3,$ are the normal and shearing forces applied at the shear centre and $S_1, S_2, S_3,$ are the twisting couple and the bending torques, evaluated with respect to the shear centre, as well. The coefficients a, g_j, b_j ($j=2, 3$), c, h are the extension, shear, bending, torsion, warping stiffness, respectively, k accounts for the gap between warping and torsion, while d, f_j ($j=2, 3$), g keep into account the couplings between extension and torsion, bending and torsion, warping and torsion, respectively [12, 13, 14].

In this way the virtual work density of the stress, reads

$$\delta\varphi = \varphi'\delta\varepsilon = Q_1\delta\varepsilon_{1c} + Q_2\delta\varepsilon_{2c} + Q_3\delta\varepsilon_{3c} + S_1\delta\chi_1 + S_2\delta\chi_2 + S_3\delta\chi_3 + \tau\delta\alpha + \mu\delta\eta \tag{6}$$

where the prime denotes derivative of each function with respect to its own argument.

Now, by putting

$$\begin{aligned}\mathbf{s} &= Q_1 \mathbf{i}_1 + Q_2 \mathbf{i}_2 + Q_3 \mathbf{i}_3 \\ \mathbf{S} &= S_1 \mathbf{i}_2 \wedge \mathbf{i}_3 + S_2 \mathbf{i}_3 \wedge \mathbf{i}_1 + S_3 \mathbf{i}_1 \wedge \mathbf{i}_2\end{aligned}\quad (7)$$

and using equation (6), we can write

$$\int \delta\varphi dx_1 = \int (\mathbf{s} \cdot \delta\mathbf{e}_c + \mathbf{S} \cdot \delta\mathbf{E}_c + \tau\delta\omega + \mu\delta\eta) dx_1 \quad (8)$$

which, when the variations are interpreted as spatial velocity fields, coincides with the expression of the (virtual) internal power (15) in [6]. This means that the equilibrium equations underlying the present formulation are the (18) and (12)₅ of [6].

3 Bifurcation analysis

Let us consider a system of hyperelastic beams acted upon by external conservative loads, whose total potential energy can be written in the form

$$\pi(u, \lambda) = \pi(u, \epsilon(u), \lambda) = \int (\varphi(\epsilon(u)) - \lambda u) dx_1 \quad (9)$$

λ being the load parameter.

The condition of equilibrium, obtained by requesting $\pi(u, \epsilon, \lambda)$ to be stationary, can be written as

$$\begin{aligned}\sigma\delta\epsilon - \lambda\delta u &= \sigma e'(u)\delta u - \lambda\delta u = 0 \quad \forall\delta u \\ \sigma &= \varphi'(\epsilon) = s(\epsilon) \\ \epsilon &= e(u)\end{aligned}\quad (10)$$

where a prime stands for differentiation of a function with respect to its own argument.

Equations (10), supplied with appropriate boundary conditions, give a *nonlinear* Boundary Value Problem whose solutions are the equilibrium states of the structure.

3.1 Asymptotic solution

Let us assume, now, that (10) admits two solution branches: $(u^f(\tau), \lambda^f(\tau))$ and $(u^b(t), \lambda^b(t))$, t and τ being real parameters, that we call *fundamental* and *bifurcated*, respectively. In addition, we assume that the two branches intersect at a point where $\tau = \tau_s$, $t = 0$, so that $(u^f(\tau_s) = u^b(0), \lambda^f(\tau_s) = \lambda^b(0))$

If the fundamental solution is known, we may introduce the *difference* fields

$$v = u^b - u^f \quad (11)$$

and look for the asymptotic expansion of the bifurcated solution near the bifurcation point, that is

$$\begin{aligned} v(t) &= \bar{v}_s t + \frac{1}{2} \bar{\bar{v}}_s t^2 + o(t^2) \\ \lambda(t) &= \lambda_s + \bar{\lambda}_s t + \frac{1}{2} \bar{\bar{\lambda}}_s t^2 + o(t^2) \end{aligned} \quad (12)$$

where superimposed bars denote derivatives with respect to t evaluated at $t = 0$.

In view of (11) and (12), the *nonlinear* BVP is transformed in a sequence of *linear* BVPs.

The first of them results in an eigenvalue problem whose solution gives the *critical loads* λ_s and the associated *critical modes* \bar{v}_s . The second system is non homogeneous and singular: its solvability condition gives the coefficients $\bar{\lambda}_s$ for each bifurcated path. It can now be solved for each one of the $\bar{\lambda}_s$ previously obtained. These solutions give the *secondary modes* for each one of the admissible equilibrium paths. Passing now to the third system we observe that it is non homogeneous and singular as the second one. Also in this case its solution relies on imposing a solvability condition that, in turn, gives the coefficients $\bar{\bar{\lambda}}_s$ for each bifurcated path.

3.2 Imperfection analysis

If the structure under analysis has an initial shape which is slightly different from the one assumed as reference—that we shall call *perfect*—we can identify the displacement field, say \tilde{u} , leading from the *perfect* to the *imperfect* shape.

Under the same loading process the *perfect* and the *imperfect* structures will behave in a different way, that is they must be characterized by two different total potential energy functionals.

Denoting by $\tilde{\pi}(u, \tilde{u}, \lambda)$ the total potential energy functional of the *imperfect* structure, we assume that the following relationship holds true

$$\tilde{\pi}(u, \tilde{u}, \lambda) = \pi(u, \lambda) + \psi(u, \tilde{u}, \lambda) \quad (13)$$

where, obviously, $\psi(u, \tilde{u}, \lambda)$ must be such that

$$\begin{aligned} \psi(u, 0, \lambda) &= 0 & \forall \delta u \\ \psi(0, \tilde{u}, \lambda) &= 0 & \forall \delta \tilde{u} \end{aligned} \quad (14)$$

Now, if we put

$$\tilde{u} = \zeta \tilde{u} \quad (15)$$

ζ being a real parameter, it can be proved that, in order to account for *small* initial imperfections expression (12)₂ can be recast in the form

$$\lambda(t) = \lambda_s + \bar{\lambda}_s t - (\zeta \varrho) \frac{1}{t} + o(t) \quad (16)$$

where

$$\varrho = \frac{\psi_s'^* \ddot{u} \bar{v}_s}{\widehat{\pi}_s'' \bar{v}_s^2} \quad (17)$$

Note that in (17) $'^*$ and $\widehat{}$ stand for derivative with respect to \ddot{u} and λ , respectively. Besides, $\psi_s'^*$ and $\widehat{\pi}_s''$ are evaluated at the bifurcated point of the *perfect* structures, which means that $\psi_s'^* = \psi_s'^*(u^f(\lambda_s), 0, \lambda_s)$ and $\widehat{\pi}_s'' = \widehat{\pi}_s''(u^f(\lambda_s), \lambda_s)$.

When $\bar{\lambda}_s = 0$ expression (16) changes in

$$\lambda(t) = \lambda_s + \frac{1}{2} \bar{\lambda}_s t^2 - (\zeta \varrho) \frac{1}{t} + o(t) \quad (18)$$

4 Frames postbuckling analysis

In this Section, we carry out the analysis of an L-Frame made up by channel beams arranged in two different ways and subjected to various boundary conditions. The frame is loaded by a vertical thrust (see Figure 1, where the lines of the centroids are represented).

In order to make a comparison of the results obtained, we will consider the same L-Frame analyzed by Basaglia et al. [9] in the framework of the GBT theory, whose results were kindly communicated to the writers by the authors.

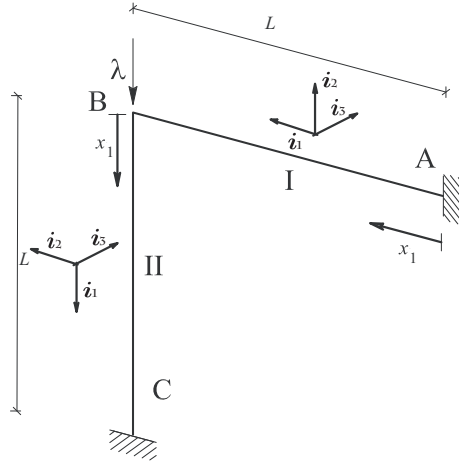


Figure 1: Two-bar frames structure.

The (U-shaped) cross-sections of the channel beams that make up the frame, have outer dimensions of 200 mm (web), 100 mm (flanges) and uniform thickness of 7 mm, $L = 5\,000$ mm.

We will consider two arrangements of the beams, that we will call Frame A and Frame B, and are shown in Figure 2.

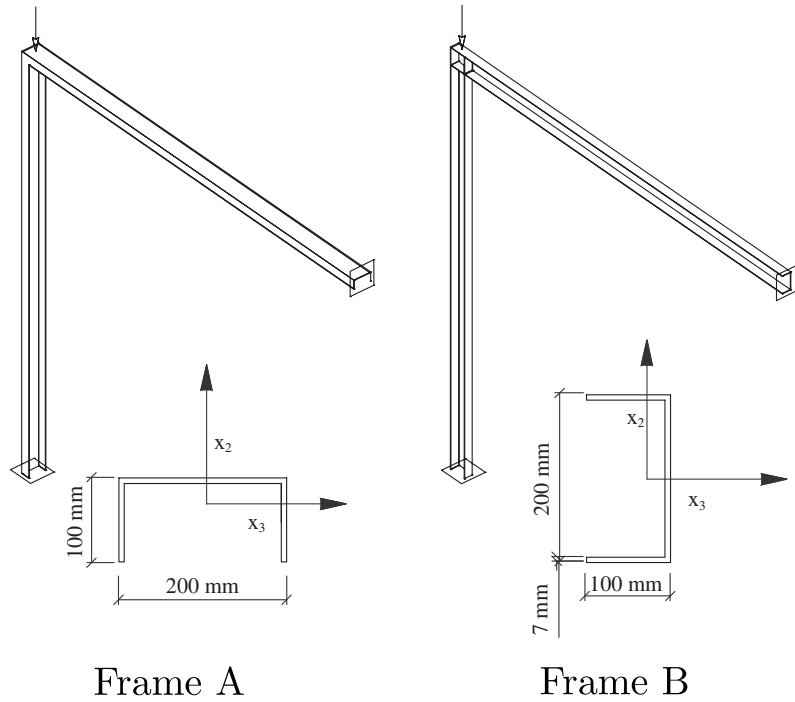


Figure 2: Two-bar frames.

The geometric and inertia quantities of the cross sections of Frame A referred to the local coordinate systems shown in Figure 2, are

$$\begin{aligned}
 a &= 2800 \text{ mm}^2 E; & c &= 45733.3 \text{ mm}^4 G; \\
 d &= 3.25323 \cdot 10^7 \text{ mm}^4 E; & h\xi^2 &= 2.04167 \cdot 10^{10} \text{ mm}^6 E; \\
 b_2 &= 1.86724 \cdot 10^7 \text{ mm}^4 E; & b_3 &= 2.92238 \cdot 10^6 \text{ mm}^4 E; \\
 g_2 &= 2800 \text{ mm}^2 G; & g_3 &= 2800 \text{ mm}^2 G \\
 f_2 &= 0; & f_3 &= -6.85417 \cdot 10^8 \text{ mm}^5 E; \\
 c_2 &= 62.5 \text{ mm}; & c_3 &= 0; .
 \end{aligned} \tag{19}$$

where E and G stand for the Young's and the shear modulus, respectively.

The geometric and inertia quantities of the cross sections of Frame B, referred to the local coordinate systems shown in Figure 2, are obtained by exchanging subscripts 2 and 3 in (19).

The following analysis is performed by assuming $E = 206 \text{ GPa}$, $G = 79 \text{ GPa}$ and $k \rightarrow \infty$. Besides, as the cross sections have one axis of symmetry, $g = 0$ [10]. The analysis will be performed for the problems listed below.

- *Case A1*

We will consider Frame A subjected to the following boundary conditions

$$\begin{array}{llll}
\mathbf{u} = \mathbf{0}, & \mathbf{R} = \mathbf{0}, & \alpha = 0, & \text{in A and C} \\
\mathbf{u}_I = \mathbf{u}_{II}, & \mathbf{R}_I = \mathbf{R}_{II}, & \alpha_I = \alpha_{II}, & \text{in B}
\end{array} \quad (20)$$

• *Case A2*

Frame A is now subjected to the same boundary conditions (20) with the additional constraint

$$\mathbf{u}_I \cdot \mathbf{i}_3 = 0. \quad \text{in B} \quad (21)$$

that prevents the out of plane displacement of node B.

• *Cases B1, B2, B3*

The attention is now turned to Frame B, subjected to the boundary conditions

$$\begin{array}{llll}
\mathbf{u} = \mathbf{0}, & \mathbf{R} = \mathbf{0}, & \alpha = 0, & \text{in A and C} \\
\mathbf{u}_I = \mathbf{u}_{II}, & \mathbf{R}_I = \mathbf{R}_{II}, & \mathbf{u}_I \cdot \mathbf{i}_3 = 0, & \text{in B}
\end{array} \quad (22)$$

plus one of the following conditions on warping transmission across the joint B,

$$\begin{array}{ll}
\text{case a} & \alpha_I = \alpha_{II} \\
\text{case b} & \alpha_I = -\alpha_{II} \\
\text{case c} & \alpha_I = \alpha_{II} = 0
\end{array} \quad (23)$$

that correspond to the three configurations of joint B shown in Figure 3 [15, 16, 17].

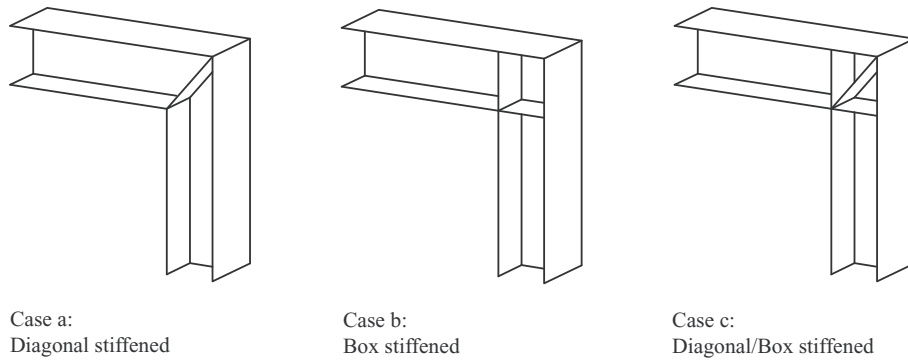


Figure 3: Configurations of the joint.

Cases B1, B2, B3 are obtained when to Frame B are imposed the boundary conditions (22) plus, in turn, (23)₁, (23)₂, (23)₃.

4.1 Buckling and postbuckling analysis

Here, following the asymptotic procedure outlined in Section 3, we analyze the initial postbuckling behaviour of the *Cases* described before.

It can easily be seen that the following fields

$$\begin{aligned}
\mathbf{u}_I^f &= \mathbf{0}, & \mathbf{R}_I^f &= \mathbf{I}, & \alpha_I^f &= 0, \\
\mathbf{e}_I^f &= \mathbf{0}, & \mathbf{E}_I^f &= \mathbf{0}, & \eta_I^f &= 0, \\
\mathbf{s}_I^f &= \mathbf{0}, & \mathbf{S}_I^f &= \mathbf{0}, & \tau_I^f &= 0, & \mu_I^f &= 0, \\
\mathbf{u}_{II}^f &= -\frac{\lambda}{a}x_1\mathbf{i}_1, & \mathbf{R}_{II}^f &= \mathbf{I}, & \alpha_{II}^f &= 0, & & (24) \\
\mathbf{e}_{II}^f &= -\frac{\lambda}{a}\mathbf{i}_1, & \mathbf{E}_{II}^f &= \mathbf{0}, & \eta_{II}^f &= 0, \\
\mathbf{s}_{II}^f &= -\lambda\mathbf{i}_1, & \mathbf{S}_{II}^f &= \lambda c_3 \mathbf{i}_3 \wedge \mathbf{i}_1 - & \tau_{II}^f &= 0, & \mu_{II}^f &= 0. \\
& & & \lambda c_2 \mathbf{i}_1 \wedge \mathbf{i}_2, & & & &
\end{aligned}$$

identify a solution branch for equations (10) for all those *Cases*. We assume this solution as the fundamental path.

Besides, for each one of the of *Cases* the first two buckling loads, the associated buckling modes and the corresponding values of the coefficients $\bar{\lambda}_s$, are determined. When $\bar{\lambda}_s = 0$ the solution to the second order equations set is also determined and the coefficients $\bar{\lambda}_s$ evaluated.

5 Numerical results

In this section the results obtained for the initial postbuckling analysis of the frames introduced before, are reported. The numerical simulations have been carried out by means of the COMSOL mutiphysics software. In order to identify the equilibrium paths that bifurcate at each one of the two critical loads considered, we refer to the features of their buckling mode. So we will call

- *out of plane flexural-torsional*: the mode in which the fields u_3, θ_2, θ_1 are largely prevailing;
- *in plane flexural-torsional*: the mode in which the fields u_2, θ_3, θ_1 are largely prevailing;
- *in plane flexural*: the mode in which the sole fields u_2, θ_3 do not vanish.

5.1 Case A1

The first case examined concerns Frame A with boundary conditions (20), which is exactly the case studied in [9], whose results are reported here in Figures 4 and 5.

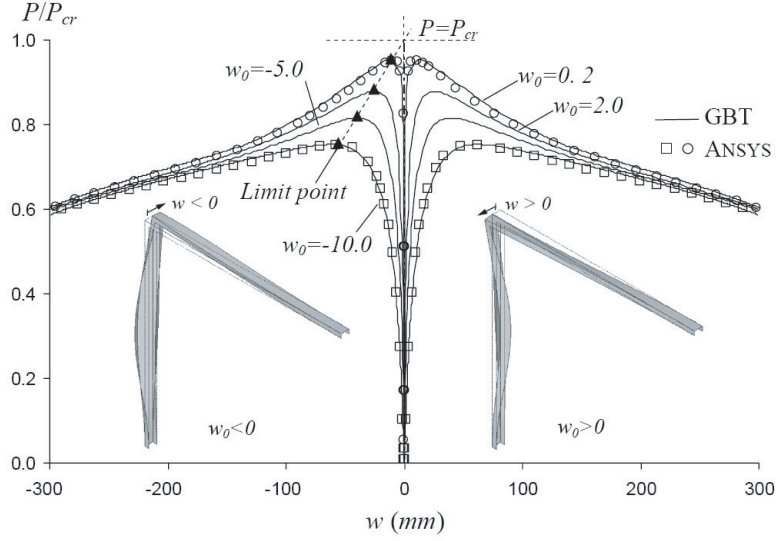


Figure 4: First buckling load: results in [9]

Note that, in order to compare the results, we have adopted the same parametrization and the same initial imperfection fields of [9]. That is w , w_0 in Figure 4 correspond to u_{3B} , U_3 in Figure 6; θ , θ_0 in Figure 5 correspond to θ_{3B} , Θ_3 in Figure 7.

The first two buckling loads, result to be

$$\begin{aligned}\lambda_s &= 6.05 \cdot 10^5 N, \\ \lambda_s &= 6.82 \cdot 10^5 N\end{aligned}\tag{25}$$

The buckling mode associated to the first buckling load is *out of plane flexural-torsional* and the relative bifurcated path results to be symmetric as $\bar{\lambda}_s = 0$.

The secondary mode adds an in plane flexural deformation and the bifurcated path results to be unstable symmetric. Figure 6 shows the equilibrium paths of the frame subject to initial imperfections having the shape of the buckling mode and amplitudes: $U_3 = 0.2, 2, 5, 10 \text{ mm}$, where U_3 stands for the out of plane displacement of joint B.

What is worth to note is that the curves in Figure 6 are very close to those in Figure 4 only for small values of the parameter. Nevertheless, the values of the limit loads of the imperfect structures are very close.

The mode associated to the second buckling is *in plane flexural*. It is of the type studied long time ago by Roorda and Chilver [18], [19] that can be considered a prototype of asymmetric postbuckling frame behaviour.

Figure 7 shows the equilibrium paths of this structure for a set of imperfections having the shape of the associated buckling mode and amplitudes: $\Theta_3 = 5 \cdot 10^{-4}, 10^{-3}, 3 \cdot 10^{-3}, 5 \cdot 10^{-3}, 10^{-2} \text{ rad}$ where Θ_3 stands for the joint rotation around an axis orthogonal to the plane of the frame.

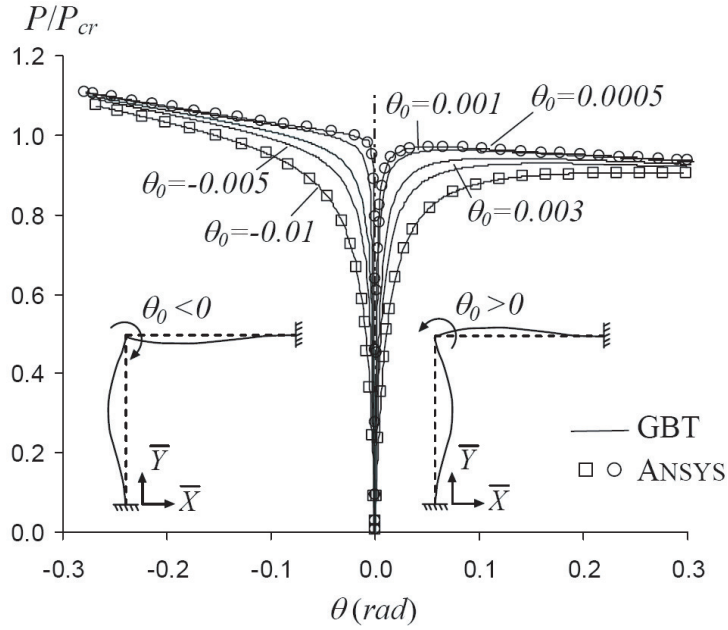


Figure 5: Second buckling load: results in [9]

It is interesting to note that in this case, the curves obtained by the authors and those in Figure 5 stand close one to the other for values of the parameter much larger than in the previous case.

Incidentally we point out that the value of the initial slope of the bifurcated path coincide with that reported in [20] that, in turn, was in very good agreement with the experiments of Roorda.

5.2 Case A2

The second case examined concerns Frame A with boundary conditions (21).

The first two buckling loads, are now

$$\begin{aligned}\lambda_s &= 6.82 \cdot 10^5 N, \\ \lambda_s &= 6.94 \cdot 10^5 N\end{aligned}\tag{26}$$

The first value, the corresponding mode and the relative value of $\bar{\lambda}_s$ are exactly the same obtained for the second bifurcated path in Section 5.1. So Figure 8 is exactly the same as Figure 7 and has been reported only for the reader's convenience.

The *out of plane flexural-torsional* mode is now associated to the second critical load and is associated to a buckling load which is now higher although very close to the lower one.

Figure 9 shows the equilibrium paths of the imperfect structure. In this case, the parametrization used in Section 5.1 cannot be adopted, as $u_{3B} = 0$. In order to show

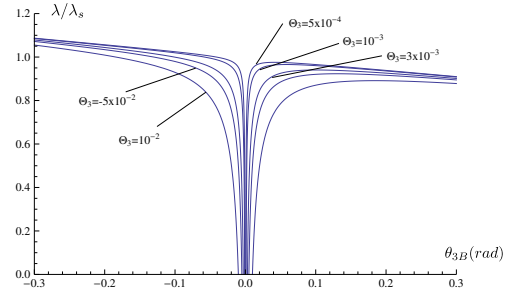
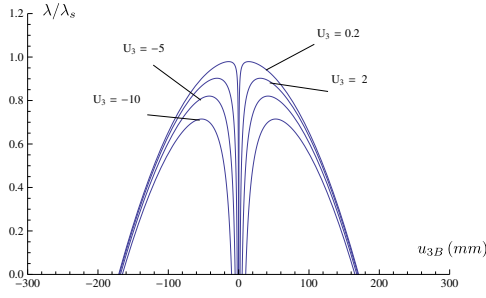


Figure 6: *Case A1* first bifurcated path Figure 7: *Case A1* second bifurcated path

results that are comparable with the previous one, we have chosen as parameter the out of plane displacement at the column midspan. It has been denoted by u_{3m} . The imperfections considered still have the shape of the buckling mode with amplitudes: $U_3 = 0.2, 2, 5, 10 \text{ mm}$. It can be seen that by imposing the constraint (21) that, of course, causes a great reduction of the out of plane sway of the frame, one obtains a double beneficial effect as the buckling load rises while the initial curvature decreases.

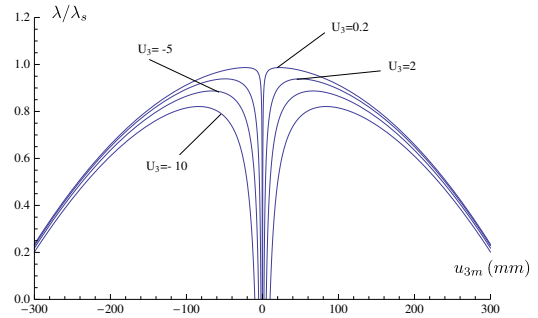
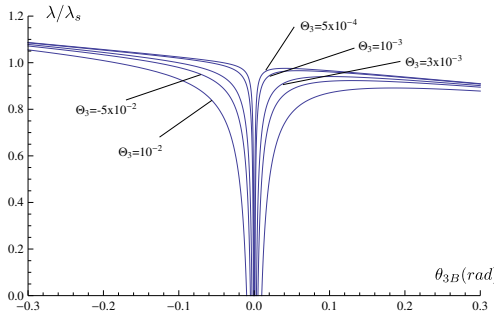


Figure 8: *Case A2* first bifurcated path Figure 9: *Case A2* second bifurcated path

Passing now to examine Frame B we recall that we will consider three cases in which the boundary conditions (22) remains the same and the warping transmission at the joint changes according to (23).

5.3 Case B1

The first case considered refers to the box stiffened joint, that is to the condition on warping transmission (23)₂.

The first two buckling loads, result to be

$$\begin{aligned}\lambda_s &= 4.87 \cdot 10^5 N, \\ \lambda_s &= 7.13 \cdot 10^5 N\end{aligned}\tag{27}$$

The buckling mode associated to the first load is *out of plane flexural-torsional*. Figure 10 shows the equilibrium paths of the structure when the load approaches this critical value, for imperfections having the shape of the associated buckling mode and amplitudes: $U_3 = 0.2, 2, 5, 10 \text{ mm}$.

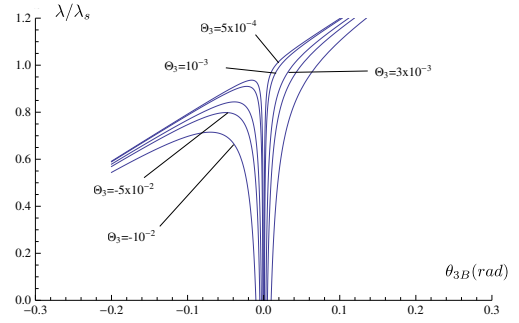
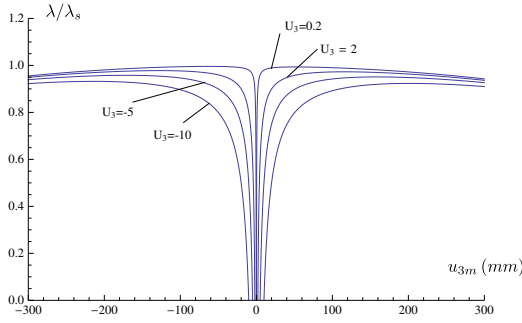


Figure 10: *Case B1* first bifurcated path Figure 11: *Case B1* second bifurcated path

The buckling mode associated to the second load is *in plane flexural-torsional*. Figure 11 shows the equilibrium paths of the structure for imperfections having the shape of the associated buckling mode and the following amplitudes: $\Theta_3 = 5 \cdot 10^{-4}, 10^{-3}, 3 \cdot 10^{-3}, 5 \cdot 10^{-3}, 10^{-2} \text{ rad}$.

The results show that the first bifurcated path is unstable symmetric even though the initial curvature is very small.

The second bifurcated path, instead, is highly asymmetric and therefore, very imperfection sensitive.

5.4 Case B2

In this case the joint is diagonally stiffened and the condition on warping transmission is $(23)_1$

The first two buckling loads are the same found for Case B1, that is

$$\begin{aligned}\lambda_s &= 4.87 \cdot 10^5 N, \\ \lambda_s &= 7.13 \cdot 10^5 N\end{aligned}\tag{28}$$

Nevertheless, the post critical behaviour of the first bifurcated path remains symmetric but with a (slight) positive initial curvature. Figure 12 shows the equilibrium paths of the structure when the load approaches this critical value, for imperfections amplitudes: $U_3 = 0.2, 2, 5, 10 \text{ mm}$.

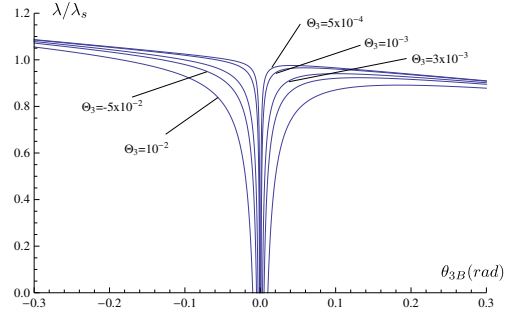
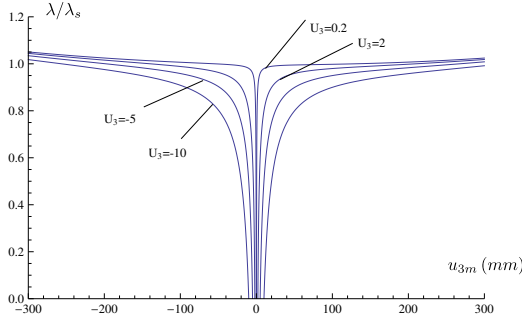


Figure 12: *Case B2* first bifurcated path Figure 13: *Case B2* second bifurcated path

The bifurcated path associated to the second load is practically the same as before. So the curves reported in Figure 13 are practically the same of those in Figure 11.

Although the initial curvature of the first bifurcated path is very small, we think that the change of its sign is, in principle, quite interesting.

5.5 Case B3

Let's pass now to consider the case of the box-diagonal stiffened joint which is modelled by the condition on warping transmission $(23)_3$.

The first two buckling loads, result to be

$$\begin{aligned}\lambda_s &= 4.87 \cdot 10^5 N, \\ \lambda_s &= 8.27 \cdot 10^5 N\end{aligned}\tag{29}$$

Nothing to say about the first bifurcated path as it corresponds to the one examined in the previous case (diagonal), that remains symmetric and stable.

Also the second bifurcated path shows the same features as before apart the fact that the associated critical load is now 16% higher.

We observe that in this case, while the stiffening of the node results in an increase of the critical load the postbuckling behaviour do not get any benefit.

6 Conclusion

A nonlinear elastic beam model that accounts for warping has been used to analyze the initial postbuckling behaviour of two L-frames subjected to various constraint conditions, by means of the asymptotic bifurcation theory.

The analysis performed show that, despite their simple shape, the frames can buckle in very different ways, depending on the beam arrangements and on the constraints

imposed. The effects of the warping transmission across the joint have also been examined.

The numerical results obtained for *Case A1* have been compared with the corresponding ones obtained by Basaglia et al. in the framework of the GBT.

The other *Cases* examined show that: a) by restraining the out of plane sway of the joint, a dangerous (although symmetric) buckling mode is eliminated; b) changing the arrangements of the beams result in a loss of the frame load carrying capacity, due to the triggering of an out of plane flexural torsional mode.

All the comparisons show that the asymptotic analysis gives information on the bifurcated paths that, even though in general can not help to know its evolution far from the bifurcated point, are sufficient to obtain a very good estimate of the load carrying capacity of the frames.

References

- [1] H. Wagner, *Verdrehung und Knickung von offenen Prolen*, 1929, translated in NACA TM 807 (1936).
- [2] R. Kappus, *Drillknicken zentrich gedruckter Stabe mit offenem Prol im elastischen Bereich*, 1937, translated in NACA TM 851 (1938).
- [3] V.Z. Vlasov, *Thin-walled elastic beams*, Jerusalem, Monson, (1961).
- [4] N.L. Rizzi, V. Varano, *The effects of warping on the postbuckling behaviour of thin-walled structures*, *Thin-Walled Structures* **49** (2011) 10911097.
- [5] N.L. Rizzi, V. Varano, *On the Postbuckling Analysis of Thin-Walled Frames*, Proceedings of the Thirteenth International Conference on Civil, Structural and Environmental Engineering Computing, B.H.V. Topping, Y. Tsompanakis, (Editors), Civil-Comp Press, Stirlingshire, UK, Paper 43, 2011. doi:10.4203/ccp.96.43
- [6] G.C. Ruta, V. Varano, M. Pignataro, N.L. Rizzi, *A beam model for the flexural-torsional buckling of thin-walled members with some applications*, *Thin-Walled Structures* **46** (2008),816–822.
- [7] W. T. Koiter, *Over de stabiliteit van het elastisch evenwicht*, Thesis, Delft 1945, translated in NASA TT F-10 vol. 833 (1967) and AFFDL Report TR 70-25 (1970).
- [8] B. Budiansky, *Theory of buckling and postbuckling behavior of elastic structures*, in: *Advances in applied mechanics* **14**, C.S. Yih, editor; New York, Academic Press, (1974).
- [9] C. Basaglia, D. Camotim, N. Silvestre, *Local, Distortional and Global Post-Buckling Analysis of Frames using Generalised Beam Theory*, Proceedings of the Tenth International Conference on Computational Structures Technology, B.H.V. Topping, J.M. Adam, F.J. Pallarés, R. Bru, M.L. Romero, (Editors), Civil-Comp Press, Stirlingshire, UK, Paper 196, 2010. doi:10.4203/ccp.93.196
- [10] N. Rizzi, A. Tatone, *Nonstandard models for thin-walled beams with a view to*

- applications*, Journal of Applied Mechanics 63, (1996), 399–403.
- [11] M. Pignataro, N.L. Rizzi, G.C. Ruta, V. Varano, *The effects of warping constraints on the buckling of thin-walled structures*, Journal of Mechanics of Materials and Structures Vol. 4 (2009), No. 10, 1711-1727 .
- [12] C. Truesdell, W. Noll, *The non-linear field theories of mechanics*, in: Handbuch der Physik III/3, New York, Springer-Verlag, (1965).
- [13] H. Møllmann, *Theory of thin-walled beams with finite displacements*, in: EUROMECH Colloquium 197, W. Pietraszkiewicz editor; New York, Springer-Verlag, (1986), 195–209.
- [14] L. M. Zubov, *Direct and Inverse Poynting Effects in Elastic Cylinders* , Doklady Physics, Vol. 46, No. 9, 675–677 (2001). Translated from Doklady Akademii Nauk, Vol. 380, No. 2, 194196 (2001).
- [15] C. Basaglia, D. Camotim, N. Silvestre, *Global buckling analysis of plane and space thin-walled frames in the context of GBT*, Thin-Walled Structures 46 (2008), 79–101.
- [16] G. S. Tong, X.X. Yan, L. Zhang, *Warping and bimoment transmission through diagonally stiffened beam-to-column joints*, Journal of Constructional Steel Research, 61 (2005), 749–763.
- [17] S. Krenk, L. Damkilde, *Warping of joints in I-beam assemblages*, Journal of Engineering Mechanics 117 No 11 (1991) 2457–2474.
- [18] J. Roorda, *Stability of structures with small imperfections*, J. Engng Mech. Div. Am. Soc. Civ. Engrs, **91**, EM 1, 87–106 (1965).
- [19] J. Roorda and A. H. Chilver, *Frame buckling: An illustration of the perturbation technique*, Int. J. Non-Linear Mech., **5**, 235–246 (1970).
- [20] N. Rizzi, A. Di Carlo, M. Pignataro, *A parametric postbuckling analysis of an asymmetric two-bar frame*, J. Struct. Mech., 8(4), 435-448 (1980).